Available online at www.sciencedirect.com
SCIENCE DIRECT®
PERGAMON
Polyhedron 22 (2003) 1157–1165
POLYHEDRON
www.elsevier.com/locate/poly

Polyoxoanion-supported pentamethylcyclopentadienylrhodium complexes: syntheses and structural characterization by EXAFS

Richard Villanneau [a], Anna Proust [a], Francis Robert [a], Françoise Villain [a,b], Michel Verdaguer [a], Pierre Gouzerh [a,*]

[a] *Laboratoire de Chimie Inorganique et Matériaux Moléculaires, UMR CNRS 7071, Université Pierre et Marie Curie, 4 Place Jussieu, 75252 Paris, Cedex 05, France*

[b] *Laboratoire d'Utilisation du Rayonnement Electromagnétique, Batiment 209d, Centre Universitaire Paris-Sud, BP 34, 91898 Orsay, Cedex, France*

Received 28 June 2002; accepted 10 December 2002

Abstract

The $[Mo_5O_{13}(OMe)_4(NO)]^{3-}$ anion either as a mixed $Na^+/n\text{-}Bu_4N^+$ or Na^+/Me_4N^+ salt reacts with $[Cp^*RhCl_2]_2$ after partial or total elimination of chloride in methanol and, sometimes, subsequent addition of bromide, to form $[\{Cp^*Rh(H_2O)\}Mo_5O_{13}(OMe)_4(NO)]^-$ isolated as a $n\text{-}Bu_4N^+$ or Me_4N^+ salt, and $[\{(Cp^*Rh)_2(\mu\text{-}X)\}Mo_5O_{13}(OMe)_4(NO)]$ (X = Cl or Br). The low-temperature rhodium K-edge extended X-ray absorption fine structure (EXAFS) data for $(n\text{-}Bu_4N)[\{Cp^*Rh(H_2O)\}Mo_5O_{13}(OMe)_4(NO)]$ and $[\{(Cp^*Rh)_2(\mu\text{-}Cl)\}Mo_5O_{13}(OMe)_4(NO)]$ have been fitted by five- and seven-shell models, respectively, and agree well with X-ray crystallographic data for $(Me_4N)[\{Cp^*Rh(H_2O)\}Mo_5O_{13}(OMe)_4(NO)]\cdot 2H_2O$ and $[\{(Cp^*Rh)_2(\mu\text{-}Br)\}Mo_5O_{13}(OMe)_4(NO)]\cdot CH_2Cl_2$. These compounds can serve as structural models for the elucidation of the bonding mode of Cp*Rh fragments in other polyoxoanion-supported rhodium(III) complexes. In that way, another compound which could not be analyzed by X-ray diffraction has been identified as an adduct of $(n\text{-}Bu_4N)_2[\{Na(MeOH)\}Mo_5O_{13}(OMe)_4(NO)]$ with $[\{(Cp^*Rh)_2(\mu\text{-}Cl)\}Mo_5O_{13}(OMe)_4(NO)]$ on the basis of EXAFS data.

Keywords: Molybdenum; Rhodium; Polyoxometalate; Organometallic chemistry; EXAFS

1. Introduction

The coordination chemistry of polyoxoanions provides soluble analogues of grafted oxide surface metal fragments [1]. The niobium-substituted polyoxotungstates *cis*-$[Nb_2W_4O_{19}]^{4-}$ and $[P_2W_{15}Nb_3O_{62}]^{9-}$ have been extensively studied by the Klemperer and Finke groups, respectively, and they have proved to be especially suitable for the formation of stable adducts with organometallic fragments [2,3]. As far as we are concerned, we have focused on the lacunary Lindqvist-type oxo-nitrosyl molybdate $[Mo_5O_{13}(OMe)_4(NO)]^{3-}$ (for short $\{Mo_5\}$) [4], which has been found to react with a variety of cations, including organic cations, e.g. $RC(NH_2)_2^+$ [5], main-group cations, e.g. Na^+ [4], Ba^{2+} and Bi^{3+} [6], f-block cations, e.g. Eu^{3+} and Ce^{4+} [6], and d-block cations, e.g. Ni^{2+} [7] and Ag^+ [8]. Regarding the reactivity of $[Mo_5O_{13}(OMe)_4(NO)]^{4-}$ towards organometallic complexes, we first concentrated on $(\eta^5\text{-}C_5Me_5)Rh(III)$ derivatives. Indeed, several polyoxoanion-supported Cp*Rh(III) complexes, including $[(Cp^*Rh)Nb_2W_4O_{19}]^{2-}$ [9], $[(Cp^*Rh)M_5O_{18}(TiCp)]^-$ (M = Mo, W) [2], $[(Cp^*Rh)P_3O_9]^-$ [10], $[(Cp^*Rh)_8\{(Mo^V_{12}O_{36})(Mo^{VI}O_4)\}]^{2+}$ [11], $[(Cp^*Rh)SiNb_3W_9O_{40}]^{5-}$ [12], $[(Cp^*Rh)P_2Nb_3W_{15}O_{62}]^{7-}$ [13] and $[(Cp^*Rh)_4V_6O_{19}]$ [14], had already been reported. In all of these adducts, the Cp*Rh unit is bound to three contiguous doubly-bridging oxygen atoms of the support. On the other hand, integrated complexes $[(Cp^*Rh)_4Mo_4O_{16}]$ [15] and $(n\text{-}Bu_4N)_2[(RhCp^*)_2Mo_6O_{20}(OMe)_2]$ [16] have been obtained by condensation of $Na_2[MoO_4]$ and $(n\text{-}Bu_4N)_2[Mo_2O_7]$ with $[Cp^*RhCl_2]_2$ in aqueous solution and in methanol, respectively. A preliminary survey of the reactivity of

* Corresponding author. Tel.: +31-1-44275562; fax: +31-1-44273841.
E-mail address: pg@ccr.jussieu.fr (P. Gouzerh).

0277-5387/03/$ - see front matter © 2003 Elsevier Science Ltd. All rights reserved.
doi:10.1016/S0277-5387(03)00040-8

$(n\text{-}Bu_4N)_2[\{Na(MeOH)\}Mo_5O_{13}(OMe)_4(NO)]$ (**1a**) towards $[Cp^*RhCl_2]_2$ in methanol has revealed the formation of several products; $(Me_4N)[\{Cp^*Rh(H_2O)\}Mo_5O_{13}(OMe)_4(NO)]\cdot 2H_2O$ (**2b**·$2H_2O$) and $[\{(Cp^*Rh)_2(\mu\text{-}Br)\}Mo_5O_{13}(OMe)_4(NO)]\cdot CH_2Cl_2$ (**3b**·CH_2Cl_2) were characterized by X-ray diffraction [17]. We report herein a more detailed investigation, including the characterization of $(n\text{-}Bu_4N)[\{Cp^*Rh(H_2O)\}Mo_5O_{13}(OMe)_4(NO)]$ (**2a**), $[\{(Cp^*Rh)_2(\mu\text{-}Cl)\}Mo_5O_{13}(OMe)_4(NO)]$ (**3a**) and $(n\text{-}Bu_4N)_2[\{Na(MeOH)\}Mo_5O_{13}4(NO)][\{(Cp^*Rh)_2(\mu\text{-}Cl)\}Mo_5O_{13}(OMe)_4(NO)]$ (**4a**) using extended X-ray absorption fine structure (EXAFS) spectroscopy. The main goal of this work was to determine if **2a** and **3a** could serve as structural models for the elucidation of the bonding mode of Cp*Rh fragments in other polyoxoanion-supported rhodium(III) complexes and ultimately in rhodium complexes bound to oxides.

2. Experimental

The oxo-nitrosyl precursors $(n\text{-}Bu_4N)_2[\{Na(MeOH)\}Mo_5O_{13}(OMe)_4(NO)]\cdot 3MeOH$ (**1a**) and $(Me_4N)_2[\{Na(H_2O)\}Mo_5O_{13}(OMe)_4(NO)]$ (**1b**) were prepared as previously reported [4]. Pentamethylcyclopentadiene (Cp*H) [18] and $[Cp^*RhCl_2]_2$ [19] were prepared according to the literature. Reagent grade solvents and starting materials ($RhCl_3\cdot xH_2O$, $AgNO_3$, Me_4NBr) were purchased from Acros Chemicals or Aldrich and used as received. Infrared spectra were recorded from KBr pellets on a Bio-Rad FT 165 spectrometer. Electronic spectra were recorded on a Shimadzu UV-2101 spectrophotometer. ^{95}Mo NMR spectra were recorded on an AM 500 Bruker spectrometer at 32.6 MHz using conventional 10 mm o.d. sample tubes. Chemical shifts were referenced to an external aqueous alkaline Na_2MoO_4 solution. Elemental analyses were performed by the Service Central d'Analyse of the CNRS (Vernaison, France).

2.1. Synthesis of $(n\text{-}Bu_4N)[\{Cp^*Rh(H_2O)\}Mo_5O_{13}(OMe)_4(NO)]$ (**2a**)

$AgNO_3$ (0.084 g, 0.5 mmol) was added to a solution of $[Cp^*RhCl_2]_2$ (0.078 g, 0.125 mmol) in MeOH (10 ml) and the mixture was stirred for approximately 30 min. Then the precipitate of AgCl was filtered off, washed with 5 ml of methanol, and the filtrate was dropped into a solution of **1a** (0.34 g, 0.25 mmol) in methanol (5 ml). The mixture was refluxed for 7 h during that time **2a** deposited as an orange–brown solid. Red crystals of **2a**·*x*MeOH formed from the dark red filtrate upon cooling overnight at −40 °C. Yield for $(n\text{-}Bu_4N)[\{Cp^*Rh(H_2O)\}Mo_5O_{13}(OMe)_4(NO)]$: 0.185 g (55%). IR (KBr, cm^{-1}): 1635s, 1065s, 1035sh, 930s, 895s, 845s, 695br. UV–Vis (MeOH): λ_{max}, nm (ε_{max}, $l\,mol^{-1}\,cm^{-1}$) 410 (3820), 380 (3480), 275 (20 000), 240 (33 460). ^{95}Mo NMR (323 K, MeOH/d_6-acetone) 84 (s, Mo^{VI}, 4 Mo), 831 (s (br) Mo^{II}, 1 Mo). *Anal.* Found: C, 26.83; H, 4.87; Mo, 35.99; N, 2.07; Rh, 7.95. Calc. for $C_{30}H_{65}Mo_5N_2O_{19}Rh$: C, 26.88; H, 4.89; Mo, 35.79; N, 2.09, Rh, 7.68.

2.2. Synthesis of $(Me_4N)[\{Cp^*Rh(H_2O)\}Mo_5O_{13}(OMe)_4(NO)]$ (**2b**)

This compound was similarly prepared from $(Me_4N)_2[\{Na(H_2O)\}Mo_5O_{13}(OMe)_4(NO)]$ (**1b**). However, the sample of **1b** used in preliminary studies later proved to contain some Me_4NBr. $AgNO_3$ (0.042 g, 0.25 mmol) was added to a solution of $[Cp^*RhCl_2]_2$ (0.039 g, 0.062 mmol) in MeOH (5 ml) and the mixture was stirred for 30 min, afterwards AgCl was filtered off, washed with 5 ml of methanol, and the filtrate was dropped into a solution of **1b** (0.13 g, 0.125 mmol) in methanol (20 ml). A small amount of an orange–red precipitate formed upon reflux of the mixture for 7 h. The solid was collected and the filtrate was set aside at room temperature. Red needles of $[(RhCp^*)_2(\mu\text{-}Br)_3][\{Cp^*Rh(H_2O)\}Mo_5O_{13}(OMe)_4(NO)]$ (**2c**) formed within 3 weeks. Platelet-like red crystals of $(Me_4N)[\{Cp^*Rh(H_2O)\}Mo_5O_{13}(OMe)_4(NO)]\cdot 2H_2O$ (**2b**·$2H_2O$) were obtained 1 month later.

2.3. Synthesis of $[\{(Cp^*Rh)_2(\mu\text{-}Cl)\}Mo_5O_{13}(OMe)_4(NO)]$ (**3a**) and $(n\text{-}Bu_4N)_2[\{Na(MeOH)\}Mo_5O_{13}(OMe)_4(NO)][\{(Cp^*Rh)_2(\mu\text{-}Cl)\}Mo_5O_{13}(OMe)_4(NO)]$ (**4a**)

$AgNO_3$ (0.064 g, 0.375 mmol) was added to a solution of $[Cp^*RhCl_2]_2$ (0.078 g, 0.125 mmol) in MeOH (10 ml). After stirring for 30 min the precipitate of AgCl was filtered off and washed with 5 ml of methanol. The filtrate was dropped into a solution of **1a** (0.17 g, 0.125 mmol) in methanol (5 ml), which resulted in the precipitation of an orange solid. The mixture was refluxed for 4 h and the red precipitate (**3a**) was filtered off, then washed with methanol. Then the filtrate was cooled and allowed to stand at room temperature. Dark red crystals of **4a** were collected after a few days. Yield for $[\{(Cp^*Rh)_2(\mu\text{-}Cl)\}Mo_5O_{13}(OMe)_4(NO)]$: 0.038 g (22% based on Mo). **3a**: IR (KBr, cm^{-1}): 1630s, 1065s, 1040sh, 940s, 865s, 850sh, 700br. UV (CH_2Cl_2): λ_{max}, nm (ε, $l\,mol^{-1}\,cm^{-1}$) 425 (7940), 260 (39 500). ^{95}Mo NMR (323 K, CH_2Cl_2/d_6-acetone) δ, ppm 106 (s, Mo^{VI}, 4 Mo). *Anal.* Found: C, 21.29; H, 3.12; N, 0.98. Calc. for $C_{24}H_{42}ClMo_5NO_{18}Rh_2$: C, 21.30; H, 3.13; N, 1.03. Yield for $(n\text{-}Bu_4N)_2[\{Na(MeOH)\}Mo_5O_{13}(OMe)_4(NO)][\{(Cp^*Rh)_2(\mu\text{ - }Cl)\}Mo_5O_{13}(OMe)_4(NO)]$: 0.105 g (62% based on Mo). **4a**: IR (KBr, cm^{-1}): 1615s, 1060s, 1040sh, 925s, 895s, 867s, 850sh, 690br. UV–Vis

(MeOH): λ_{max}, nm (ε, $l\,mol^{-1}\,cm^{-1}$) 410 (6920), 375 (sh, 5960), 280 (sh, 35 440), 240 (61 760). *Anal.* Found: C, 27.55; H, 4.75; Cl, 1.21; Mo, 37.00; N, 2.24; Na, 0.93; Rh, 8.02. Calc. for $C_{61}H_{130}ClMo_{10}NaN_4O_{37}Rh_2$: C, 26.79; H, 4.79; Cl, 1.30; Mo, 35.07; N, 2.05; Na, 0.84; Rh, 7.05.

2.4. Synthesis of [{(Cp*Rh)$_2$(μ-Br)}Mo$_5$O$_{13}$(OMe)$_4$(NO)] (**3b**)

$AgNO_3$ (0.126 g, 0.75 mmol) was added to a solution of $[Cp^*RhCl_2]_2$ (0.117 g, 0.188 mmol) in MeOH (5 ml), and the solution was stirred for approximately 30 min. AgCl was then filtered off and washed with 5 ml of methanol. The filtrate was dropped into a solution of **1b** (0.13 g, 0.125 mmol) and Me_4NBr (0.058 g, 0.375 mmol) in 20 ml of methanol. The resulting red solution was refluxed for 6 h to yield **3b** as a red precipitate which was filtered off and washed with methanol. Yield for [{(Cp*Rh)$_2$(μ-Br)}Mo$_5$O$_{13}$(OMe)$_4$(NO)]: 0.1 g. Octahedral crystals of **3b**·CH_2Cl_2 suitable for X-ray analysis were obtained upon recrystallization from CH_2Cl_2. **3b**: IR (KBr, cm^{-1}): 1630s, 1065s, 1040sh, 940s, 855s, 695br. *Anal.* Found: Br, 5.11; Mo, 33.74; Rh, 14.28. Calc. for $C_{24}H_{42}BrMo_5NO_{18}Rh_2$: Br, 5.72; Mo, 34.31; Rh, 14.72.

2.5. Synthesis of (n-Bu$_4$N)$_2$[{Na(MeOH)}Mo$_5$O$_{13}$(OMe)$_4$(NO)][{(Cp*Rh)$_2$(μ-Br)}Mo$_5$O$_{13}$(OMe)$_4$(NO)] (**4b**)

$AgNO_3$ (0.042 g, 0.25 mmol) was added to a solution of $[Cp^*RhCl_2]_2$ (0.039 g, 0.0625 mmol) in MeOH (5 ml) and the mixture was stirred for 30 min, afterwards AgCl was filtered off and washed with 5 ml of methanol. The filtrate was dropped into a solution of **1a** (0.34 g, 0.25 mmol) and NBu_4Br (0.04 g, 0.125 mmol) in 5 ml of methanol. The red solution was refluxed for 16 h to give a red precipitate (**4b**) which was filtered off and washed with methanol. Yield for (*n*-Bu$_4$N)$_2$[{Na(MeOH)}Mo$_5$O$_{13}$(OMe)$_4$(NO)][{(Cp*Rh)$_2$(μ-Br)}Mo$_5$O$_{13}$(OMe)$_4$(NO)]: 0.116 g (34%). **4b**: IR (KBr, cm^{-1}): 1630s, 1065s, 1040sh, 940s, 855s, 695br. *Anal*. Found: C, 26.49; H, 4.88; N, 2.20. Calc. For $C_{61}H_{130}BrMo_{10}NaN_4O_{37}Rh_2$: C, 26.36; H, 4.71; N, 2.02.

2.6. X-ray absorption studies

EXAFS measurements were performed at the rhodium K edge (23 220 eV) on the XAS 13 beam line of the DCI storage ring at LURE (Orsay), operating at 1.85 GeV with an average ring current of 300 mA. The incident beam was monochromatized by a double Ge(4 0 0) crystal. The energy calibration was checked using a Rh metal foil reference. EXAFS spectra were recorded in transmission mode using argon filled ionization chambers and at low-temperature (10 K) with a liquid-helium cryostat. Each spectrum was acquired ten times with 3 eV steps and an integration time of 2 s per point. The samples were ground and homogeneously dispersed in cellulose pellets.

The EXAFS data analysis was performed with the 'EXAFS pour le Mac' package [20]. The EXAFS signal $k\chi(k)$ is extracted from the data by using a linear preedge background, a combination of polynomials and spline atomic absorption background and the normalisation procedure of Lengeler–Eisenberger [21]. The pseudo-radial distribution functions are given by the Fourier transforms (FT) calculated on $w(k)k^3\chi(k)$ where $w(k)$ is a Kaiser-Bessel window with a smoothness parameter equal to 3. The k limits are equal to 2.6–15 $Å^{-1}$ ($\Delta k = 12.4$ $Å^{-1}$). The FT are calculated and presented without phase correction. The quality of the fits between the Fourier filtered shells $k\chi_{exp}(k)$ and the theoretical curve $k\chi_{th}(k)$ is evaluated by an agreement factor ρ (%) equal to $\Sigma[k\chi_{exp}(k)-k\chi_{th}(k)]^2/\Sigma[k\chi_{exp}(k)]^2$. On the other hand, we used the FEFF7 code [22] to check the presence of multiple scattering and to calculate the amplitude and phase functions $A_j(k,\pi)$ and $\phi_{i,j}(k)$ from model compounds ($[RhCp^*Cl_2]_2$ and **2a**).

3. Results and discussion

3.1. Syntheses

Polyoxoanion-supported pentamethylcyclopentadienylrhodium complexes can often be obtained by the reaction of $[Cp^*RhCl_2]_2$ with polyoxometalates in non-aqueous solvents. For example, (*n*-Bu$_4$N)$_2$[(Cp*Rh)Nb$_2$W$_4$O$_{19}$] has been obtained as a two-diastereomer mixture by reacting $[Cp^*RhCl_2]_2$ with (*n*-Bu$_4$N)$_4$[Nb$_2$W$_4$O$_{19}$] in CH_2Cl_2 [9]. However, the solvated complex $[Cp^*Rh(NCMe)_3]^{2+}$, which can be conveniently prepared by reaction of $[Cp^*RhCl_2]_2$ with $AgPF_6$ in acetonitrile, is more reactive than $[Cp^*RhCl_2]_2$. Regarding the specific case of $[Mo_5O_{13}(OMe)_4(NO)]^{3-}$, we observed that **1a** sometimes reacts with $[Cp^*RhCl_2]_2$ in refluxing methanol to give a brick-red precipitate (**5a**) which transforms into **3a** upon recrystallization in CH_2Cl_2. However, the reaction was unreproducible and **5a** could not be fully characterized. Owing to the instability of $[Mo_5O_{13}(OMe)_4(NO)]^{3-}$ in CH_3CN where it transforms into $[Mo_6O_{18}(NO)]^{3-}$ [23], use of CH_3CN was avoided and a solvated complex, presumably $[Cp^*Rh(MeOH)_3]^{2+}$, was generated by treating $[Cp^*RhCl_2]_2$ with the appropriate amount of $AgNO_3$ in methanol. This procedure allowed partial or complete removal of chloride depending on the amount of $AgNO_3$, and its

possible replacement with bromide. The 1:1 complex $[\{Cp^*Rh(H_2O)\}Mo_5O_{13}(OMe)_4(NO)]^-$ was preferably obtained in the absence of halide and isolated as tetrabutylammonium (**2a**) and tetramethylammonium (**2b**) salts. In addition it could be obtained in low yield as $[(RhCp^*)_2(\mu\text{-}Br)_3][\{Cp^*Rh(H_2O)\}Mo_5O_{13}(OMe)_4(NO)]$ (**2c**). The 2:1 complex $[\{(Cp^*Rh)_2(\mu\text{-}Cl)\}Mo_5O_{13}(OMe)_4(NO)]$ (**3a**) was obtained when three-quarters of chloride had been eliminated. However, another compound (**4a**) which later proved to be an adduct of **1a** and **3a**, was also obtained using this procedure. The bromide analogues **3b** and **4b** were similarly obtained after complete removal of chloride and addition of the appropriate amount of bromide as *n*-Bu_4NBr or Me_4NBr, respectively.

3.2. Crystal structures

The crystal structure analyses of **2b**·$2H_2O$ and **3b**·CH_2Cl_2 were previously reported [17], and only a brief account of the results will be given here in order to provide a basis for the interpretation of EXAFS data. The $[\{Cp^*Rh(H_2O)\}Mo_5O_{13}(OMe)_4(NO)]^-$ anions in **2b**·$2H_2O$ (Fig. 1) and the $[\{(Cp^*Rh)_2(\mu\text{-}Br)\}Mo_5O_{13}(OMe)_4(NO)]$ molecules in **2b**·CH_2Cl_2 (Fig. 2) display crystallographically imposed C_s-*m* symmetry. Selected bond distances and angles are given in Table 1. The subscripts 'ax' and 'eq' can be used to distinguish between the two kinds of terminal oxo ligands in $[Mo_5O_{13}(OMe)_4(NO)]^{3-}$. The Cp*Rh fragment in **2b**·$2H_2O$ is bonded to two adjacent axial ligands and rhodium achieves an 18-electron configuration with a molecule of water. Such a coordination mode was unprecedented for cyclopentadienylrhodium derivatives of polyoxometalates. Indeed all the previously characterized complexes contained Cp*Rh fragments attached to a triangle of bridging oxo ligands [9–14]. However, the species $[\{Cp^*RhCl_2\}Nb_2W_4O_{19}]^{4-}$, where the polyoxoanion binds to rhodium through one of its ONb oxygen atoms, has been proposed as an intermediate in the formation of $[\{Cp^*Rh\}Nb_2W_4O_{19}]^{2-}$ by reaction of $[Cp^*RhCl_2]_2$ with $[Nb_2W_4O_{19}]^{4-}$ [9]. In **3b** the $\{Mo_5\}$ support acts as a bridging ligand: one Cp*Rh fragment is attached to each pair of axial ligands and the two rhodium centres are further linked by a bromide ligand. The Mo–O bonds are slightly but significantly lengthened upon binding of the oxygen atoms to rhodium, which results in a shortening of the *trans* Mo–O bonds. Although the Mo–O bond lengths involving the nitrosyl-bearing Mo centre are only weakly affected, the

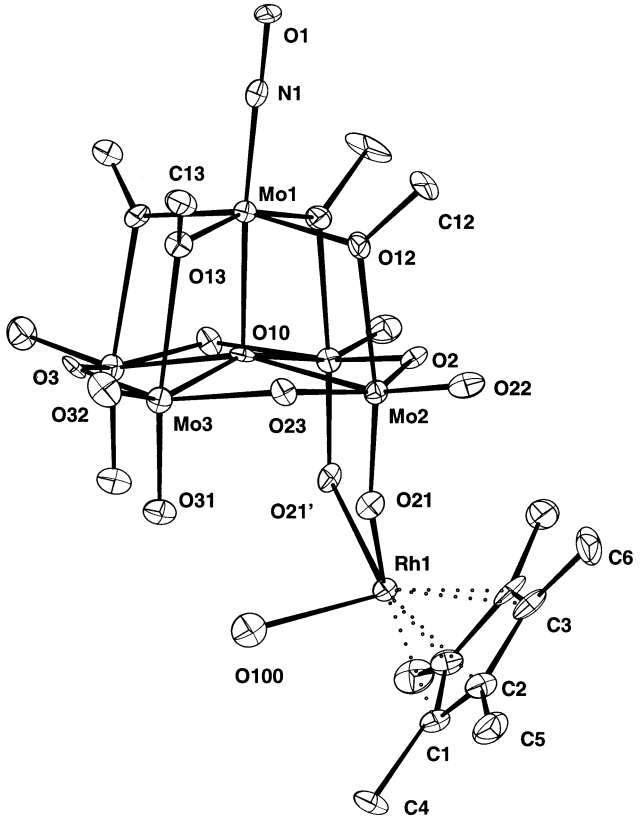

Fig. 1. View [29] of the anion of **2b**·$2H_2O$ [17]. Thermal ellipsoids are shown at the 20% probability level.

Table 1
Selected bond lengths (Å) for the anion of **2b**·$2H_2O$ and for **3b**·CH_2Cl_2

Anion of **2b**·$2H_2O$		**3b**·CH_2Cl_2	
Mo(1)–N(1)	1.77(3)	Mo(1)–N(1)	1.78(1)
Mo(1)–O(10)	2.14(2)	Mo(1)–O(10)	2.123(9)
Mo(1)–O(12)	2.01(2)	Mo(1)–O(12)	2.021(8)
Mo(1)–O(13)	1.94(2)	Mo(1)–O(13)	1.985(8)
Mo(2)–O(10)	2.34(2)	Mo(2)–O(10)	2.323(7)
Mo(2)–O(12)	2.20(1)	Mo(2)–O(12)	2.215(8)
Mo(2)–O(21)	1.75(2)	Mo(2)–O(2)	1.911(6)
Mo(2)–O(22)	1.66(2)	Mo(2)–O(21)	1.753(8)
Mo(2)–O(23)	1.86(2)	Mo(2)–O(22)	1.688(8)
Mo(2)–O(2)	1.88(1)	Mo(2)–O(23)	1.910(7)
Mo(3)–O(10)	2.32(2)	Mo(3)–O(10)	2.334(7)
Mo(3)–O(13)	2.33(1)	Mo(3)–O(13)	2.243(8)
Mo(3)–O(23)	1.93(2)	Mo(3)–O(23)	1.918(7)
Mo(3)–O(31)	1.70(2)	Mo(3)–O(3)	1.911(6)
Mo(3)–O(32)	1.69(2)	Mo(3)–O(31)	1.740(8)
Mo(3)–O(3)	1.89(1)	Mo(3)–O(32)	1.681(8)
Mo(2)–O(21)	1.75(2)	N(1)–O(1)	1.16(2)
Mo(2)–O(22)	1.66(2)	Rh(2)–O(21)	2.101(8)
Mo(3)–O(31)	1.70(2)	Rh(2)–Br(1)	2.539(2)
Mo(3)–O(32)	1.69(2)	Rh(2)–C(20)	2.13(2)
N(1)–O(1)	1.21(4)	Rh(2)–C(21)	2.12(1)
Rh(1)–O(21)	2.11(2)	Rh(2)–C(22)	2.15(1)
Rh(1)–C(1)	2.15(4)	Rh(3)–O(31)	2.119(8)
Rh(1)–C(2)	2.12(3)	Rh(3)–Br(1)	2.550(3)
Rh(1)–C(3)	2.16(3)	Rh(3)–C(30)	2.09(5)
Rh(1)–O(100)	2.13(3)	Rh(3)–C(31)	2.11(3)
		Rh(3)–C(32)	2.14(3)
		Rh(3)–C(130)	2.14(5)
		Rh(3)–C(131)	2.11(3)
		Rh(3)–C(132)	2.12(3)

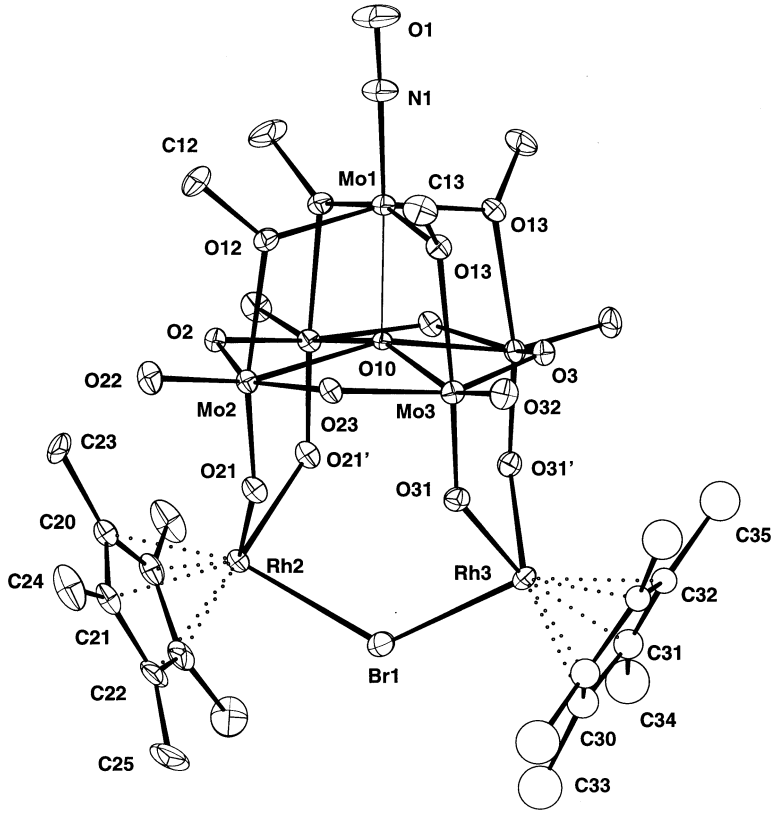

Fig. 2. View [29] of the anion of **3b**·CH_2Cl_2 [17]. Thermal ellipsoids are shown at the 20% probability level.

pattern of bond length alternation is clearly apparent in $[\{Cp^*Rh(H_2O)\}Mo_5O_{13}(OMe)_4(NO)]^-$. On the contrary a symmetrical pattern is observed for $[\{(Cp^*Rh)_2(\mu\text{-}Br)\}Mo_5O_{13}(OMe)_4(NO)]$. Comparison of the Mo–O(Rh) bond lengths with the $Mo–O_{eq}$ bond lengths shows that the former retain significant double character so that $[\{Cp^*Rh(H_2O)\}Mo_5O_{13}(OMe)_4(NO)]^-$ and $[\{(Cp^*Rh)_2(\mu\text{-}Br)\}Mo_5O_{13}(OMe)_4(NO)]$ are best described as polyoxoanion-supported complexes. As a matter of fact, no genuine $\{Mo_5\}$-incorporated complex has been characterized so far.

3.3. Infrared spectroscopy

The infrared spectra of compounds **1**–**4** show similar patterns characteristic of the $[Mo_5O_{13}(OMe)_4(NO)]^{3-}$ anion: these are the band assigned to ν(NO) in the range 1615–1630 cm^{-1}, two bands assigned to ν(O–C) of methoxo ligands at approximately 1040 cm^{-1}, several bands assigned to $\nu(Mo{=}O_t)$ in the range 955–830 cm^{-1}, and one band assigned to $\nu(Mo–O_b–Mo)$ at approximately 700 cm^{-1}. In the course of our systematic study of the coordination behaviour of the $\{Mo_5\}$ anion, we have found that the pattern of $\nu(Mo{=}O_t)$ bands is indicative of the coordination mode: three bands are observed when the $\{Mo_5\}$ anion acts as a bidentate ligand while only two bands are observed when the four axial oxo ligands are symmetrically bonded to one or two metal centres [6]. Thus the IR spectra of compounds **2** (three bands at 855, 895 and 935 cm^{-1}) and **3** (two bands at 855 and 940 cm^{-1}) are consistent with the crystal structures of **2b** and **3b**. Although this was not recognized until EXAFS studies had been completed, it is now apparent that **4a** displays a pattern of bands that could be explained by superimposition of the respective bands of **1a** and **3a**.

3.4. Electronic spectroscopy

The UV–Vis spectra of **2a** and **4a** in methanol display a set of four broad charge-transfer bands at approximately 410, 380 (sh), 275 (sh) and 240 nm. By comparison with **1a** and $[Cp^*RhCl_2]_2$, the first two bands are assigned to the Cp*Rh fragments and the fourth to an oxygen-to-molybdenum charge transfer transition. The origin of the band at 275 nm is unclear. The band assigned to the $d_{xz}, d_{yz} \rightarrow d_{xy}$ transition within the $\{Mo(NO)\}^{3+}$ unit which is well defined and observed for most derivatives including the $\{Mo_5\}$ unit [23] is masked by the broad band at 410 nm. The spectrum of complex **3a** has been recorded in CH_2Cl_2 and a single band is observed at 425 nm, the bands at higher energy being masked by the absorption of the solvent.

3.5. Mo NMR

The ^{95}Mo NMR spectra of **2a** and **3a** were recorded at 323 K in methanol/d_6-acetone and in dichloromethane/d_6-acetone, respectively. By comparison with **1a** [23], the spectrum of $[\{(Cp^*Rh)_2(\mu\text{-}Cl)\}Mo_5O_{13}(OMe)_4(NO)]$ (**3a**) should display two lines in intensity ratio 4:1 assuming that the solid-state structure of the complex is retained in solution. However, a single peak is observed at 106 ppm, in the typical range for under-ivatized and unreduced polyoxomolybdates, while the expected highly deshielded resonance from the $Mo^{II}(NO)$ group could not be observed, possibly because of its broadness. A single but asymmetric peak was also observed for the less symmetrical anion $[\{Cp^*Rh(H_2O)\}Mo_5O_{13}(OMe)_4(NO)]^-$ of **2a**, instead of the expected two-lines (1:1) pattern for the Mo(VI) centres. In this case, the Mo^{II} (NO) signal was observed at 831 ppm.

3.6. EXAFS analysis

The characterization of solid-oxide supported rhodium organometallic compounds is of fundamental interest in the field of heterogeneous catalysis. In this regard, EXAFS spectroscopy has emerged as one of the important techniques able to provide local structural information [24]. In contrast, there are only a few examples of EXAFS analysis of polyoxometalates [25–27]. As far as Rh derivatives are concerned, Rh K-edge but also V K- and Mo K-edge analyses were previously carried out respectively on SiO_2-grafted $[\{(\eta^3\text{-}C_4H_7)_2Rh\}_2V_4O_{12}\}]$ and $[(Cp^*Rh)_4V_6O_{19}\}]$ complexes [26] and on cubane-type integrated clusters [27].

In the present study, compounds **2a** and **3a** were used as models for the structural characterization of **4a**. X-ray absorption spectra were recorded for compounds **2a**, **3a**, **4a** and $[RhCp^*Cl_2]_2$ in the solid state. Data were collected at low temperature (10 K) in order to take advantage of the reduction of the Debye-Waller factors.

First, the EXAFS signal of **2a** was modelled by using the FEFF7 code and the structural parameters derived from the single-crystal X-ray analysis of the related NMe_4^+ salt (**2b**). Fig. 3 shows the modulus and the imaginary part of the FT of the experimental and calculated EXAFS signals of **2a** with (Fig. 3(a)) and without (Fig. 3(b)) multiple scattering. The calculated FT spectrum of **2a** including multiple scattering is in close agreement with the experimental data. The assignment of the peaks is straightforward: the first shell at approximately 2.13 Å comprises the five nearest carbon atoms of the Cp* ligand and the three nearest oxygen atoms (the coordinated water molecule and the two axial oxo ligands O(21) and O(21)′ of the $\{Mo_5\}$ unit in Fig. 1). The second main peak arises from the Mo shell (Mo(2) at 3.64 Å). The shoulder observed on the second peak could be attributed to the contribution of the second carbon atoms (C*) of the Cp* ligand (average distance 3.26 Å) and to some multiple scattering pathways. The peak at 5.22 Å should correspond to Mo(3), but experimental and calculated data do not fit very well above 4.5 Å.

For **2a**, only the Mo(2) shell was affected by multiple scattering until 4.5 Å. Furthermore, we have checked by using the FEFF7 code that, in the calculated FT of the EXAFS signal of **3b**, (i) the Rh(3) and Br(1) shells can clearly be distinguished from the other peaks and that (ii) neither the Rh(3) nor the Br(1) shell are affected by multiple scattering. Consequently, it may be inferred that for the present series of compounds the uncertainty due to neglecting multiple scattering is concerned only with the Mo(2) shell.

Second, the experimental EXAFS signals of **3a** and **4a** and the moduli of their FT were compared to those of **2a** (Fig. 4). Data for **3a** and **4a** are rather similar but different from those of **2a**. The three main peaks for **2a**, corresponding to the C+O, Mo(2) and Mo(3) shells, are also observed for **3a** and **4a**. Two further peaks at

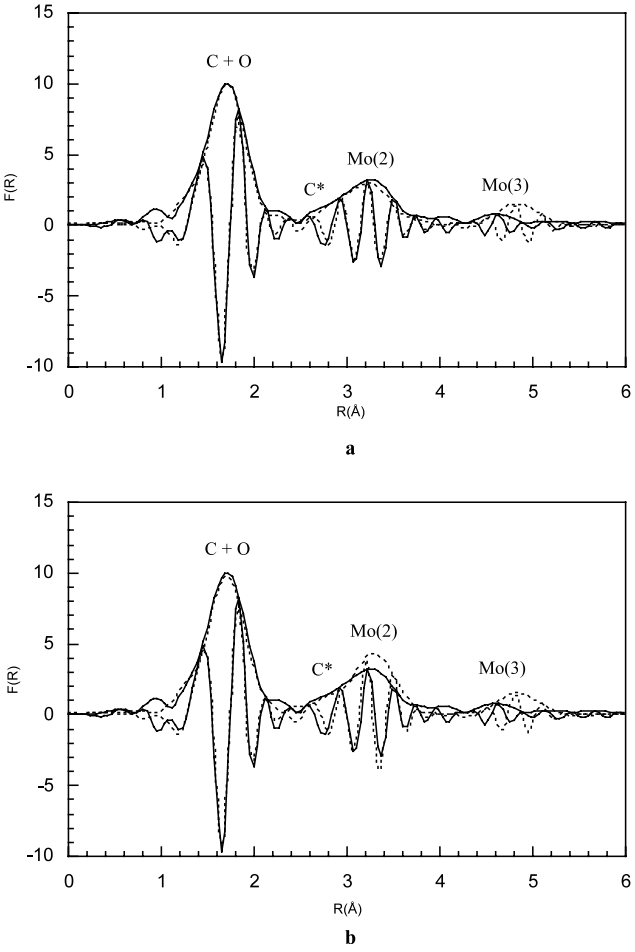

Fig. 3. Modulus and imaginary part of the FT of the experimental (solid lines) and calculated (dotted lines) EXAFS signals of **2a** with (a) and without (b) multiple scattering.

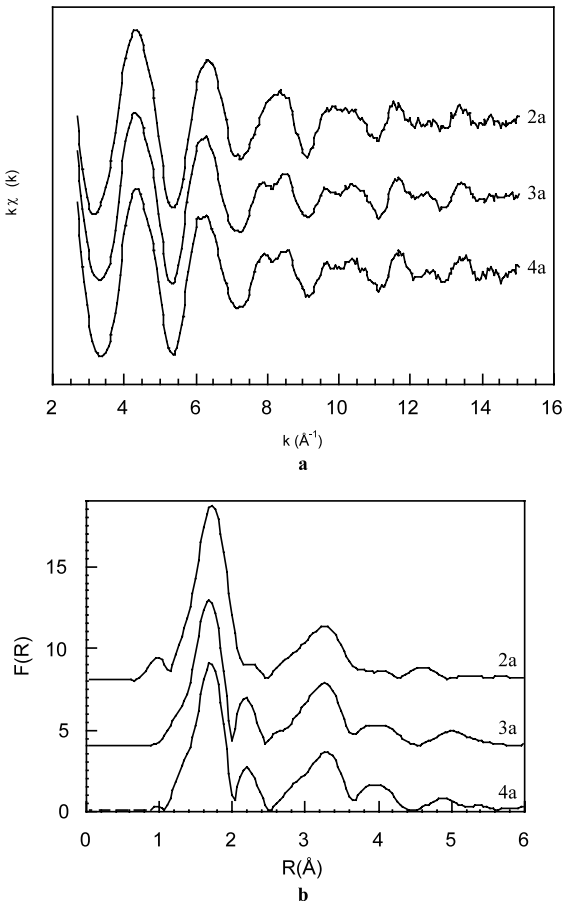

Fig. 4. Experimental EXAFS signals (a) and the moduli of their FT (b) of **2a** (bottom), **3a** (middle) and **4a** (top).

approximately 2.4 and 4.2 Å are attributed to the Rh···Cl and Rh···Rh contributions arising from a Rh–Cl–Rh unit.

Third, the EXAFS signals of **3a** and **4a** were simulated by using the program Round Midnight [20]. The experimental and simulated $F(R)$ moduli of the EXAFS signals are shown in Fig. 5 for **3a** (Fig. 5(a)) and **4a** (Fig. 5(b)). As shown above, only the Mo(2) shell could be affected by neglecting multiple scattering. Since the program does not allow to fit simultaneously more than five shells, fitting procedures were achieved in the following way: fitting of the carbon, oxygen and chlorine shells (filtered between 1.07 and 2.50 Å), fitting of the carbon (methyl of the Cp* ligand), Rh and Mo shells (filtered between 2.52 and 5.25 Å), and comparison of the seven-shell model with the experimental EXAFS signal. Structural parameters and agreement factors ρ (%) given in Table 2 are the ones obtained in the successive steps of the fitting procedure. S_0^2, $\lambda_j(k)$, $A_j(k,\pi)$ and $\phi_{i,j}(k)$ were extracted from model compounds using the FEFF7 code. The only significant difference in the simulations of **3a** and **4a** lies in the Rh···Rh contribution. The corresponding peak is somewhat more intense and occurs at a slightly shorter distance for **4a** (4.32 Å) than for **3a** (4.36 Å) but the difference is within the experimental error. The increased Rh···Rh contribution in **4a** is likely due to a decrease of the Debye-Waller factor. We could then assume that the bridge Rh–Cl–Rh is more rigid in **4a** than in **3a**.

In conclusion of the EXAFS study, it is clear that the environment of rhodium is the same in compounds **3a** and **4a**, which means that both compounds contain the complex $[\{RhCp^*\}_2(\mu\text{-}Cl)Mo_5O_{13}(OMe)_4(NO)]$. According to chemical analyses, **4a** would thus appear as an adduct of **1a** and **3a**. Co-crystallization of polyoxometallates is precedented [28]. The conclusion drawn from EXAFS studies has now been confirmed by IR spectroscopy. Indeed, the IR spectrum of **4a** is well fitted by a superimposition (in the same ratio) of the spectra of the precursor **1a** and of the target compound **3a**.

Table 2
Fitted structural parameters for **3a** and **4a** as determined by EXAFS at Rh K-edge

Compound	Backscatterer	N	σ (Å)	R (Å)	ΔE_0 (eV)	ρ (%)
3a	C	5	0.05	2.14	4.0	
	O	2	0.05	2.11	0	5
	Cl	1	0.05	2.45	8.0	
	C*	5	0.07	3.25	7.0	
	Mo(2)	2	0.06	3.64	−2.0	7
	Rh	1	0.06	4.36	−4.0	
	Mo(3)	2	0.07	5.30	7.0	
4a	C	5	0.05	2.14	4.0	
	O	2	0.05	2.11	0	5
	Cl	1	0.05	2.46	9.0	
	C*	5	0.06	3.25	7.0	
	Mo(2)	2	0.06	3.64	−2.0	5
	Rh	1	0.04	4.32	−4.0	
	Mo(3)	2	0.07	5.25	7.0	

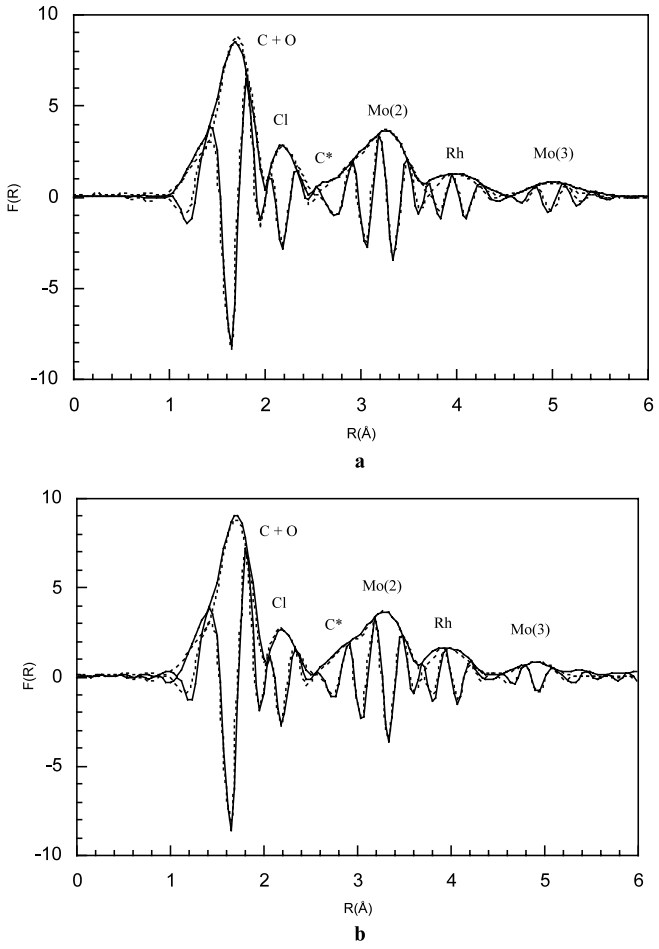

Fig. 5. Experimental (solid lines) and fitted (dotted lines) modulus and imaginary part of the EXAFS signal for **3a** (a) and **4a** (b).

4. Concluding remarks

The $[Mo_5O_{13}(OMe)_4(NO)]^{3-}$ anion as a mixed Na^+/n-Bu_4N^+ (**1a**) or Na^+/Me_4N^+ (**1b**) salt reacts with $[Cp^*RhCl_2]_2$ in methanol, after partial or total elimination of chloride and possible addition of n-Bu_4NBr or Me_4NBr, to form $[Mo_5O_{13}(OMe)_4(NO)\{Cp^*Rh(H_2O)\}]^-$ as a n-Bu_4N^+ (**2a**) or Me_4N^+ (**2b**) salt, and $[Mo_5O_{13}(OMe)_4(NO)\{(Cp^*Rh)_2(\mu\text{-}X)\}]$ (X = Cl, **3a**, X = Br, **3b**). The crystal structures of **2b**·$2H_2O$ and **3b**·CH_2Cl_2 have been determined by single-crystal X-ray diffraction methods. The accuracy of rhodium K-edge EXAFS curve fitting in the determination of the rhodium environment in **2a** and **3a** has been assessed. This allowed the identification of compound (**4a**), which could not be analyzed by X-ray diffraction, as an adduct of **1a** and **3a**. These results further demonstrate the potential of Rh K-edge EXAFS spectroscopy in the structural characterization of polyoxometalate-supported rhodium complexes and provide well-defined structural and spectroscopic models for the characterization of rhodium fragments grafted onto oxide surfaces.

5. Supporting information available

Modulus and imaginary part of the FT of the calculated EXAFS signal of **3b**.

6. Supplementary material

Details of the crystal structure investigations may be obtained from the Fachinformationszentrum Karlsruhe, Gesellschaft für wissenschaftlichtechnische Information mbH, D-W-7514 Eggenstein-Leopoldshafen 2 (FRG), on quoting the depository number CSD-56624.

Acknowledgements

We thank the CNRS and the Université Pierre et Marie Curie for supporting this work. We are grateful to Dr René Thouvenot for the ^{95}Mo NMR characterization of the complexes.

References

[1] (a) L.C.W. Baker, in: S. Kirschner (Ed.), Advances in the Chemistry of the Coordination Compounds, Macmillan, New York, 1961, p. 608;
(b) V.W. Day, W.G. Klemperer, Science 228 (1985) 533;
(c) P. Gouzerh, A. Proust, Chem. Rev. 98 (1998) 77.
[2] V.W. Day, W.G. Klemperer, in: M.T. Pope, A. Müller (Eds.), Polyoxometalates: From Platonic Solids to Anti-retroviral Activity, Kluwer, Dordrecht, 1994, p. 87 (and references therein).
[3] T. Nagata, M. Pohl, H. Weiner, R.G. Finke, Inorg. Chem. 36 (1997) 1366 (and references therein).
[4] P. Gouzerh, Y. Jeannin, A. Proust, F. Robert, Angew. Chem., Int. Ed. Engl. 28 (1989) 1363.
[5] S.-G. Roh, A. Proust, F. Robert, P. Gouzerh, J. Cluster Sci. 7 (1996) 593.
[6] R. Villanneau, A. Proust, F. Robert, P. Gouzerh, J. Chem. Soc., Dalton Trans. (1999) 421.
[7] R. Villanneau, A. Proust, F. Robert, P. Veillet, P. Gouzerh, Inorg. Chem. 38 (1999) 4981.
[8] R. Villanneau, A. Proust, F. Robert, P. Gouzerh, Chem. Comm. (1998) 1491.
[9] C.J. Besecker, V.W. Day, W.G. Klemperer, M.R. Thompson, J. Am. Chem. Soc. 106 (1984) 4125.
[10] C.J. Besecker, V.W. Day, W.G. Klemperer, Organometallics 4 (1985) 564.
[11] H.K. Chae, W.G. Klemperer, D.E. Paez-Loyo, V.W. Day, T.A. Eberspacher, Inorg. Chem. 31 (1992) 3187.
[12] R.G. Finke, M.W. Droege, J. Am. Chem. Soc. 106 (1984) 7274.
[13] (a) D.J. Edlund, R.J. Saxton, D.K. Lyon, R.G. Finke, Organometallics 7 (1988) 1692;
(b) K. Nomiya, C. Nozaki, M. Kaneko, R.G. Finke, M.J. Pohl, J. Organomet. Chem. 505 (1995) 23.

[14] (a) H.K. Chae, W. Klemperer, V.W. Day, Inorg. Chem. 28 (1989) 1423;
(b) K. Isobe, A. Yagasaki, Acc. Chem. Res. 26 (1993) 524.
[15] Y. Hayashi, K. Toriumi, K. Isobe, J. Am. Chem. Soc. 110 (1988) 3666.
[16] S. Takara, T. Nishioka, I. Kinoshita, K. Isobe, Chem. Commun. (1997) 891.
[17] A. Proust, P. Gouzerh, F. Robert, Angew. Chem., Int. Ed. Engl. 32 (1993) 115.
[18] C.M. Fendrick, L.D. Schertz, E.A. Mintz, T.J. Marks, Inorg. Synth. 29 (1992) 193.
[19] R.G. Ball, W.A.G. Graham, D.M. Hernekey, J.K. Hoyano, A.D. McMaster, S.B. Mattson, S. Michel, Inorg. Chem. 29 (1990) 2023.
[20] A. Michalowitz, EXAFS pour le MAC, Logiciels pour la chimie, Ed. Société Française de Chimie, Paris, 1991.
[21] B. Lengeler, P. Eisenberger, Phys. Rev. B 21 (1980) 4507.
[22] S.I. Zabinsky, J.J. Rehr, J.J. Ankudinov, R.C. Albers, M.J. Eller, Phys. Rev. B 52 (1995) 2995.
[23] A. Proust, P. Gouzerh, F. Robert, Inorg. Chem. 32 (1993) 5291.
[24] (a) Y. Iwasawa, Adv. Catal. 35 (1987) 187;
(b) H.H. Lamb, B.C. Gates, H. Knözinger, Angew. Chem., Int. Ed. Engl. 27 (1988) 1127;
(c) K. Asakura, K. Kitamura-Brando, K. Isobe, H. Arakawa, Y. Iwasawa, J. Am. Chem. Soc. 112 (1990) 3242;
(d) S.A. Vierkötter, C.E. Barnes, T.L. Hatmaker, J.E. Penner-Hahn, C.M. Stinson, B.A. Huggins, A. Benesi, P. Ellis, Organometallics 10 (1991) 803;
(e) S.L. Scott, J.-M. Basset, J. Mol. Catal. 86 (1994) 5.
[25] (a) T. Miyanaga, N. Matsubayashi, T. Fukumoto, K. Yokoi, I. Watanabe, K. Murata, S. Ikeda, Chem. Lett. (1988) 487;
(b) T. Miyanaga, T. Fujikawa, N. Matsubayashi, T. Fukumoto, K. Yokoi, I. Watanabe, S. Ikeda, Bull. Chem. Soc. Jpn 62 (1989) 1791;
(c) J. Evans, M. Pillinger, J.M. Rummey, J. Chem. Soc., Dalton Trans. (1996) 2951;
(d) A.R. Siedle, New J. Chem. 13 (1989) 719;
(e) A.R. Siedle, C.G. Markell, P.A. Lyon, K.O. Hodgson, A.L. Roe, Inorg. Chem. 26 (1987) 219.
[26] K. Takahashi, M. Yamagushi, T. Shido, H. Ohtani, K. Isobe, M. Ichikawa, J. Chem. Soc., Chem. Commun. (1995) 1301.
[27] Y. Imada, T. Shido, R. Ohnishi, K. Isobe, M. Ichikawa, Catal. Lett. 38 (1996) 101.
[28] A. Proust, R. Thouvenot, M. Chaussade, F. Robert, P. Gouzerh, Inorg. Chim. Acta 224 (1994) 81.
[29] L.J. Pearce, D.J. Watkin, CAMERON: Chemical Crystallography Laboratory, University of Oxford, Oxford, 1996.